

1 Fe–TPP Coordination Network with Metalloporphyrinic Neutral 2 Radicals and *Face-to-Face* and *Edge-to-Face* π – π Stacking

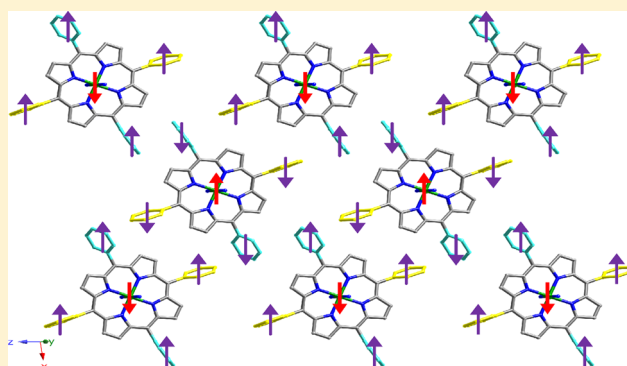
3 Arkaitz Fidalgo-Marijuan,[†] Gotzone Barandika,^{*,‡} Begoña Bazán,[†] Miren Karmele Urriaga,[†] Luis Lezama,[§]
4 and María Isabel Arriortua[†]

5 [†]Departamento de Mineralogía y Petrología and [§]Departamento de Química Inorgánica, Facultad de Ciencia y Tecnología,
6 Universidad del País Vasco (UPV/EHU), Apartado 644, 48080 Bilbao, Spain

7 [‡]Departamento de Química Inorgánica, Facultad de Farmacia, Universidad del País Vasco (UPV/EHU), Paseo de la Universidad 7,
8 01006 Vitoria-Gasteiz, Spain

9 **S** Supporting Information

10 **ABSTRACT:** Compound $([\text{FeTPPbipy}]^{\bullet})_n$ (TPP = *meso*-tetra-
11 phenylporphyrin and bipy = 4,4'-bipyridine) is the first example
12 of a Fe–TPP–bipy coordination network, and it consists of 1D
13 polymers packed through *face-to-face* and *edge-to-face* π – π
14 interactions. The compound has been investigated by means of X-ray
15 diffraction, IR, Mössbauer, UV–visible, and EPR spectroscopies,
16 thermogravimetry, magnetic susceptibility measurements, and
17 quantum-mechanical density functional theory (DFT) and time-
18 dependent DFT calculations. The chemical formula for this
19 compound can be confusing because it is compatible with Fe^{II}
20 and TPP²⁻ anions. However, the spectroscopic and magnetic
21 properties of this compound are consistent with the presence of
22 low-spin Fe^{III} ions and $[\text{FeTPPbipy}]^{\bullet}$ neutral radicals. These
23 radicals are proposed to be formed by the reduction of metalloporphyrin, and the quantum-mechanical calculations are consistent
24 with the fact that the acquired electrons are located on the phenyl groups of TPP.



25 ■ INTRODUCTION

26 Metalloporphyrins are one of the cornerstones on which the
27 existence of life is based because major biochemical, enzymatic,
28 and photochemical functions depend on the special properties of
29 the tetrapyrrolic macrocycle.¹ Thus, porphyrin catalysts are well-
30 known to be highly efficient for oxidative reactions,² and during
31 the last years, great effort has been devoted to the immobilization
32 of distinct types of catalysts on solid surfaces,^{3–5} with porphyrins
33 also having been investigated in this field.^{6–16} Thus, these com-
34 pounds can also be used for coordination networks where the
35 assembly of metalloporphyrinic structural units can be achieved
36 by coordination bonds and other weaker cohesion forces.^{17,18}
37 There are many examples of metalloporphyrinic three-
38 dimensional (3D) frameworks, but most of them consist of the
39 crystallization of monomeric complexes, with the cohesion forces
40 being hydrogen bonds and π stacking. In fact, if thinking of high
41 dimensionality in terms of the formation of coordination
42 polymers, metalloporphyrins exhibit important limitations.
43 To illustrate this point, the case of *meso*-tetraphenylporphyrin
44 (TPP) can be cited. CSD research indicates the existence of
45 monomers, dimers, trimers, and other types of aggregates.
46 However, the highest dimensionality achieved with pyridyl
47 ligands connected on axial positions for octahedral specimens
48 corresponds to one-dimensional (1D) coordination polymers,
49 and just seven of them have been prepared so far.^{19–24} It is also
50 worth mentioning that none of them has iron (Fe) as the metal

center. In fact, as far as we are aware, the highest dimensionality
51 found for Fe–TPP–dipyridyl systems consists of dimers. How-
52 ever, it must be pointed out that there are two previous examples
53 in the literature for 1D Fe–TPP polymers with cyanide-based
54 ligands.^{25,26}

The work herein presented was inspired by previously
56 reported metalloporphyrinic frameworks exhibiting bipyridyl
57 ligands.^{27–34} Our intention was the synthesis of high-dimensional
58 frameworks in which metalloporphyrins play two roles: as
59 building blocks in porous networks and as catalysts immobilized in
60 the pores. We still have not achieved this goal, but instead we have
61 synthesized and characterized the compound $([\text{FeTPPbipy}]^{\bullet})_n$,
62 where bipy is 4,4'-bipyridine (bipy). The compound exhibits 1D
63 coordination polymers that crystallize in a 3D framework in which
64 both *face-to-face* and *edge-to-face* π stacking of the phenyl groups
65 provide stability to the lattice. The main interest of this com-
66 pound lies in the fact that it is the first Fe–TPP–bipy compound
67 characterized so far. Additionally, the special characteristics of
68 this compound have produced an intricate discussion based on
69 an exhaustive characterization [X-ray diffraction, IR, Mössbauer,
70 UV–visible, and EPR spectroscopies, thermogravimetry, mag-
71 netic susceptibility measurements, and quantum-mechanical
72

Received: March 26, 2013

73 density functional theory (DFT) and time-dependent DFT
74 (TD-DFT) calculations].

75 ■ EXPERIMENTAL SECTION

76 **Materials.** All solvents and chemicals were used as received from reliable
77 commercial sources. The reagents 5,10,15,20-tetraphenylporphyriniron(III)
78 chloride (FeTPP-Cl) and 4,4'-bipyridine (bipy; 98%) and the solvent
79 *N,N*-dimethylformamide (DMF; 99.8%) were purchased from Sigma-
80 Aldrich Co.; absolute ethanol was purchased from Panreac.

81 **Physicochemical Characterization Techniques.** The IR spec-
82 trum was collected on a JASCO FT/IR-6100 spectrometer at room
83 temperature in the range of 4000–400 cm^{-1} in KBr pellets (1% of the
84 sample). C, H, and N elemental analyses were measured using a Euro EA
85 3000 elemental analyzer. UV–visible diffuse-reflectance measurements
86 were carried out on a Cary 5000 UV–visible–near-IR spectropho-
87 tometer in the range of 200–2500 nm. Thermogravimetric analyses
88 were carried out using a NETZSCH STA 449F3 thermobalance. A
89 crucible containing 10 mg of sample was heated at 5 $^{\circ}\text{C min}^{-1}$ in the
90 temperature range of 30–500 $^{\circ}\text{C}$. Mössbauer spectra were obtained at
91 room temperature using a constant-acceleration Mössbauer spectrom-
92 eter with a $^{57}\text{Co/Rh}$ source. The velocity calibration was done using a
93 metallic Fe foil. Electron paramagnetic resonance (EPR) spectra were
94 measured with a Bruker ESP-300 spectrometer operating at X band and
95 equipped with a nitrogen and helium cryostat. Magnetic susceptibility
96 measurements were measured in the range of 4–300 K with a Quantum
97 Design SQUID MPMS-7T magnetometer.

98 **X-ray Structure Determination.** Prismatic dark-blue single
99 crystals of $([\text{FeTPPbipy}]^*)_n$ with dimensions given in Table 1 were

performed by full-matrix least squares based on F^2 , using the 108
SHELXL-97 program.³⁶ Anisotropic thermal parameters were used for
109 all non-H atoms (Figure S1, Supporting Information). All H atoms
110 connected to the aromatic rings (C–H 0.95 Å) were fixed geometrically
111 and were refined using a riding model with common isotropic dis-
112 placements. Brief crystal data are listed in Table 1. (See Tables S1–S4,
113 Supporting Information, for bond distances and angles, atomic
114 coordinates, and anisotropic displacement.) 115

■ RESULTS AND DISCUSSION

116
117 **Synthesis of $([\text{FeTPPbipy}]^*)_n$.** FeTPP-Cl (7 mg, 0.01 mmol),
118 bipy (9.4 mg, 0.06 mmol), and 40 μL of NaOH (3M) were added
119 to a mixture of DMF (3 mL) and ethanol (1 mL) in a small
120 capped vial, sonicated to ensure homogeneity, and heated to
121 120 $^{\circ}\text{C}$ for 48 h, following by slow cooling to room temperature
122 at 2 $^{\circ}\text{C h}^{-1}$, yielding diffraction-quality dark-blue prismatic
123 crystals. Anal. Calcd for $\text{C}_{54}\text{H}_{36}\text{FeN}_6$: C, 78.64; H, 4.39; N,
124 10.18%. Found: C, 78.45(8); H, 4.31(10); N, 9.86(6). $\nu_{\text{max}}/\text{cm}^{-1}$:
125 3051, 3022, and 2964 [$\text{C}(\text{sp}^2)\text{H}$], 1600–1440 (CC), 1348 (CN),
126 1204 and 1070 (bipy), 1000 (FeTPP), 750 (CH) (Figure S2,
127 Supporting Information).

128 **Crystal Structure.** The crystal structure of $([\text{FeTPPbipy}]^*)_n$
129 was determined by means of single-crystal X-ray diffraction. The
130 structure consists of 1D coordination polymers extending
131 along the [010] direction, where metalated porphyrins are
132 axially bonded to two bipy ligands (Figure 1).

133 The resulting octahedral coordination sphere exhibits bond
134 angles and distances that are typical for these types of com-
135 pounds (Table 2).³⁷ These coordination polymers crystallize
136 as shown in Figure 2. The connections between chains take place
137 through *edge-to-face* π stacking along the [10–1] direction
138 (centroid-to-centroid distance of 3.662 Å and angle of 83.94 $^{\circ}$).
139 Additionally, there is a *face-to-face* π stacking along the [101]
140 direction (centroid-to-centroid distance 5.067 Å and angle
141 0.02 $^{\circ}$). Therefore, the cohesion between 1D coordination poly-
142 mers is based on a robust network of π bonds.

143 In principle, the chemical formula could be interpreted in
144 terms of the presence of Fe^{II} and TPP^{2-} ions. However, as ex-
145 plained below, the behavior of $([\text{FeTPPbipy}]^*)_n$ is consistent
146 with the presence of Fe^{III} . Therefore, because no further de-
147 protonation is observed for the organic ligands, reduction of
148 TPP^{2-} must be assumed to maintain neutrality.^{38,39}

149 Distortion of the porphyrin was analyzed by the normal-
150 coordinate structural decomposition method developed by
151 Shelnut et al.,^{40,41} indicating a low saddle-type distortion
152 (*sad*, B_{2u}). The contribution of this type of distortion (0.5967) to
153 the total displacements is 67%, a, usual feature on low-spin
154 iron(III) porphyrins.⁴²

155 It is worth mentioning that, as far as we are aware, $([\text{FeTPPbipy}]^*)_n$
156 is the first Fe–TPP–dipyridyl coordination network exhibiting 1D
157 polymers, and it has been formed by the assembly of neutral radical
158 units. More details about the latter will be discussed below.

159 **Purity of the Measured Samples.** In order to determine
160 the purity of the samples used for further characterization, the
161 grinding effect on single crystals has been evaluated by means of
162 X-ray diffraction. The results (Figure S3, Supporting Informa-
163 tion) indicate that a significant rate of amorphization takes place.
164 Taking this into consideration, magnetic susceptibility measure-
165 ments and UV–visible spectroscopy were performed by using
166 nonground single crystals introduced into a capillary in order to
167 guarantee the purity of the sample. Unfortunately, the crystal
168 features for $([\text{FeTPPbipy}]^*)_n$ were absolutely inadequate for the

Table 1. Crystallographic Data for $([\text{FeTPPbipy}]^*)_n$

compound	$([\text{FeTPPbipy}]^*)_n$
formula	$\text{C}_{54}\text{H}_{36}\text{FeN}_6$
fw, g mol $^{-1}$	824.74
cryst syst	monoclinic
space group	$\text{C2}/c$ (No. 15)
<i>a</i> , Å	21.6833(8)
<i>b</i> , Å	11.0827(4)
<i>c</i> , Å	17.6206(6)
β , deg	97.354(3)
<i>V</i> , Å 3	4199.6(3)
<i>Z</i>	4
$\rho_{\text{obs}}/\rho_{\text{calc}}$ g cm $^{-3}$	1.309(5), 1.304
<i>F</i> (000)	1712
μ , mm $^{-1}$	0.405
crystal size, mm	0.34 × 0.077 × 0.072
abs corm	analytical
radiation λ , Å	0.71073
temperature, K	100(2)
reflns collected, unique	10334, 3907 ($R_{\text{int}} = 0.04$)
limiting indices	$-26 \leq h \leq 26$, $-7 \leq k \leq 13$, $-21 \leq l \leq 19$
refinement method	full-matrix least squares on F^2
final <i>R</i> indices [$I > 2\sigma(I)$] ^a	$R1 = 0.0351$, $wR2 = 0.0714$
<i>R</i> indices (all data) ^a	$R1 = 0.0513$, $wR2 = 0.0738$
GOF on F^2	0.909
parameters/restraints	279/0

$$^a R1 = [(|F_o| - |F_c|)]/|F_o|. wR2 = [w|F_o|^2 - |F_c|^2]/[w(|F_o|^2)^2]^{1/2}.$$

100 selected under a polarizing microscope and mounted on MicroMounts.
101 Single-crystal X-ray diffraction data were collected at 100 K on an
102 Xcalibur 2 automatic diffractometer with graphite-monochromated Mo
103 $K\alpha$ radiation ($\lambda = 0.71073$ Å). The Lorentz polarization and absorption
104 corrections were made with the diffractometer software, taking into
105 account the size and shape of the crystals.³⁵ The structure was solved
106 in the monoclinic space group $\text{C2}/c$ by direct methods with the
107 *SHELXS-97* program.³⁶ Refinement of the crystal structure was

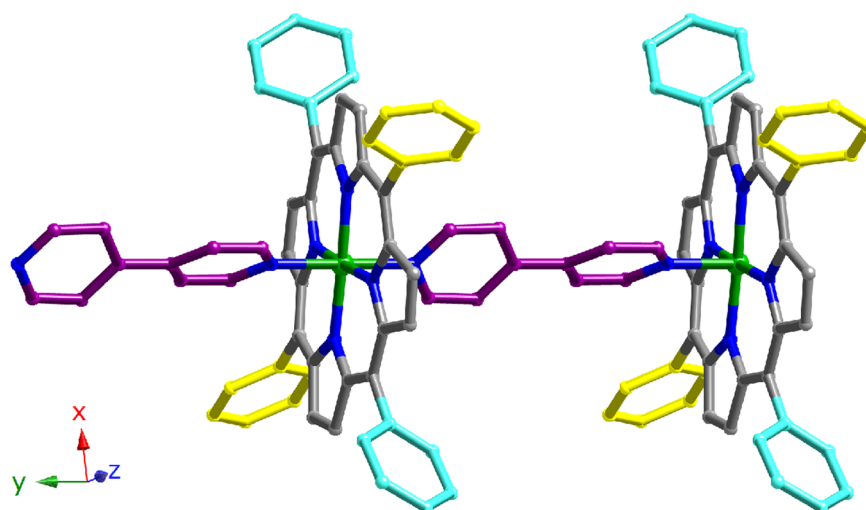


Figure 1. 1D coordination polymers extending along the [010] direction for $([\text{FeTPPbipy}]^*)_n$. Color code: green, Fe; blue, N; gray, yellow, turquoise, C(porphyrin); purple, C(bipy). H atoms are omitted for clarity.

Table 2. Selected Bond Angles (deg) and Distances (Å) for $([\text{FeTPPbipy}]^*)_n$ (Distances in Bold)^a

Fe	Octahedron $[\text{FeN}_6]$					
	N1	N1 ⁱ	N2	N2 ⁱ	N3	N4
N4	88.46(4)	88.46(4)	91.16(4)	91.16(4)	180	1.998(2)
N3	91.54(4)	91.54(4)	88.84(4)	88.84(4)	1.985(2)	
N2 ⁱ	90.14(6)	89.92(6)	177.69(8)	1.996(1)		
N2	89.92(6)	90.14(6)	1.996(1)			
N1 ⁱ	176.93(8)	1.983(1)				
N1	1.983(1)					

^aSymmetry code: $i, -x, y, -z + 1/2$.

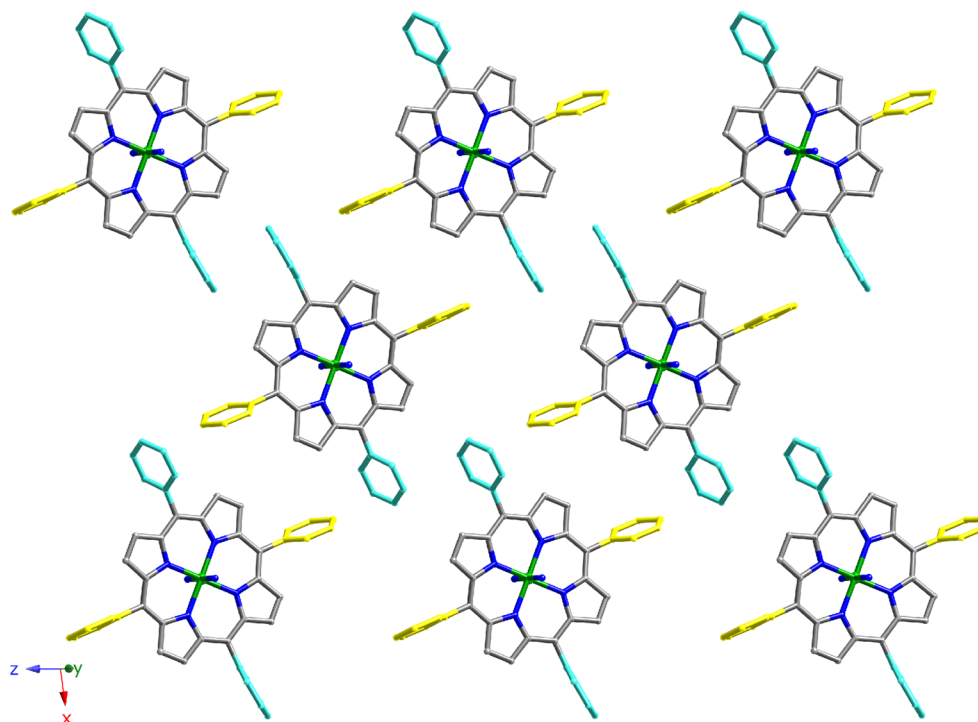


Figure 2. View of a (101) plane for $([\text{FeTPPbipy}]^*)_n$. Color codes are the same as those in Figure 1. The bipy ligands and H atoms are omitted for clarity. *Face-to-face* π stacking occurs between the turquoise phenyl groups, and *edge-to-face* π stacking occurs between the turquoise and yellow phenyl groups.

169 performance of EPR and Mössbauer spectroscopies on single
170 crystals.

UV–Visible (Diffuse-Reflectance) Spectroscopy. UV– 171
visible spectroscopy was performed on nonground single 172

173 crystals, and as observed in Figure 3a, the spectrum exhibits
174 a Soret band (γ) at 377 nm and Q bands (β and α) at 517 and

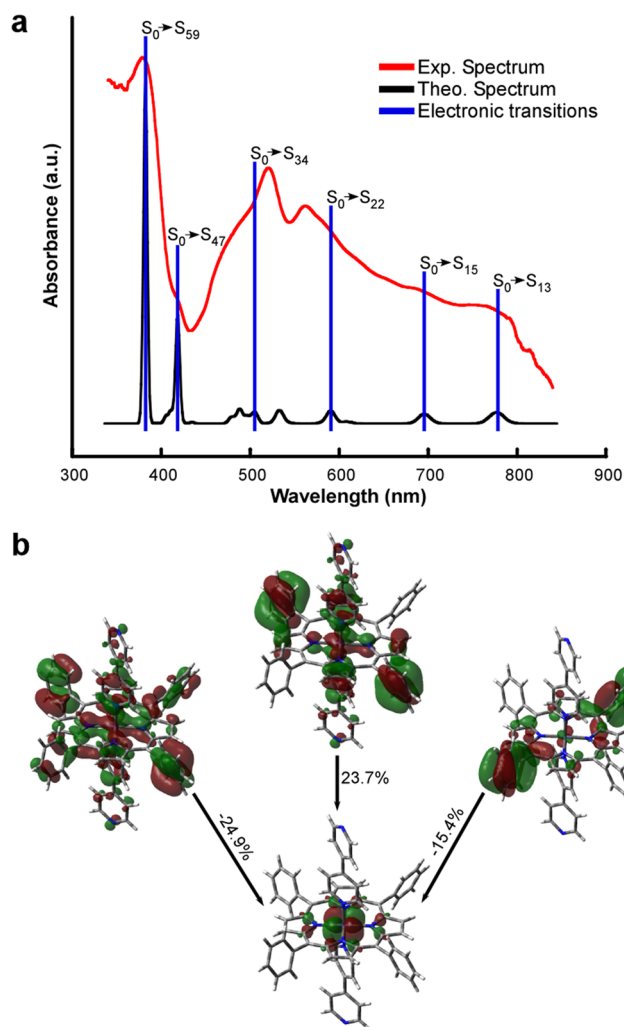


Figure 3. (a) Experimental and theoretical UV–visible spectra for $([\text{FeTPPBipy}]^{\bullet})_n$ and (b) molecular orbitals involved in the S_0 – S_{59} transition.

175 557 nm, respectively. The fact that the Soret band is blue-shifted
176 and reduced in intensity compared to typical six-coordinate low-
177 spin ferric porphyrin complexes^{25,43} is justified by assuming the
178 presence of a radical species.^{44,45} The low-spin iron(III) por-
179 phyrin characteristic L_1 and L_2 bands⁴⁶ appear at 815(sh) and
180 770 nm, respectively. A broad and weak band at 690 nm is in
181 accordance with the presence of a porphyrinic radical.⁴⁴ These
182 results were compared with the theoretical spectra (Figure 3a)
183 obtained by TD-DFT calculations, performed by means of
184 *Gaussian 03*⁴⁷ (B3LYP^{48,49} functional and 6-31G valence). In
185 addition to the good concordance between both spectra, the
186 most remarkable fact is that the molecular orbitals involved in the
187 Soret transition (S_0 – S_{59}) represent an important charge transfer
188 between the phenyl rings and the metal center (Figure 3b). This
189 fact will be mentioned below during a discussion of the magnetic
190 behavior.

191 **EPR.** X-band EPR spectroscopy was performed on ground
192 single crystals of $([\text{FeTPPBipy}]^{\bullet})_n$. As observed, the spectrum
193 shows two signals (Figure 4). The weakest of them (with g close
194 to 6) is typical for magnetically isolated Fe^{III} systems in axial

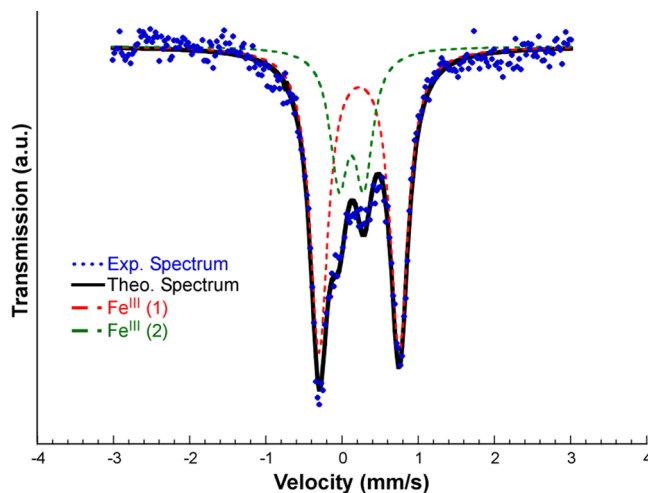


Figure 4. X-band EPR spectrum (room temperature) for $([\text{FeTPPBipy}]^{\bullet})_n$.

195 symmetry. Therefore, it is supposed to have been formed by
196 crystal grinding. Unfortunately, the fact that grinding produces
197 amorphization (Figure S3, Supporting Information) results in
198 the impossibility of identifying this second phase by X-ray
199 diffraction.

200 On the other hand, the principal signal (with g close to 2) can
201 be interpreted in terms of the following two possibilities: (a)
202 high-spin Fe^{III} ions in very low concentration in relation to the
203 bulk of the analyzed sample and (b) low-spin Fe^{III} ions with
204 either significant magnetic interactions between metal centers
205 having different orientations or interactions with free radicals.
206 In the latter case, radicals should be either delocalized or localized
207 in such a way that they could relax in a short period of time. The
208 first hypothesis does have a sense just for the case of high-spin
209 Fe^{III} ions diluted in a low-spin Fe^{II} framework. This means that
210 compound $([\text{FeTPPBipy}]^{\bullet})_n$ should contain Fe^{II} ions and that
211 there are three contributions to the signal: the compound itself,
212 the amorphous secondary phase, and a third unknown com-
213 pound. This hypothesis has been discarded by X-band EPR
214 spectroscopy at 100 K (Figure S4, Supporting Information)
215 because it shows a broadening of the signal and a rapid decrease
216 of the intensity (it mostly disappears below 50 K). This clearly
217 indicates the presence of antiferromagnetic interactions, there-
218 fore pointing to the second explanation. Thus, the second
219 explanation could just be feasible if the presence of free electrons is
220 admitted because the structural characteristics of $([\text{FeTPPBipy}]^{\bullet})_n$
221 are not compatible with significant magnetic interactions between
222 metal centers (the magnetic paths through the bipy ligands are
223 too long). As explained below, these magnetic interactions were
224 analyzed through measurements of the magnetic susceptibility
225 and by DFT calculations.

226 **Mössbauer Spectroscopy.** Mössbauer spectroscopy was
227 performed on ground single crystals. The spectrum has been
228 simulated with the *NORMOS* program⁵⁰ and indicates the
229 presence of two doublets: both of them corresponding to Fe^{III}
230 signals. The presence of two Fe^{III} centers has been explained already
231 in the EPR section, and it has been associated with amorphization
232 of the sample as a consequence of the grinding, discarding the presence
233 of a previous impurity.

234 The most significant signal is assigned to the metal ions in
235 $([\text{FeTPPBipy}]^{\bullet})_n$, while the second one is assumed to be due to
236 the secondary phase coming from grinding. Quantitative analysis
237 reveals that the sample contained 70.5% by weight correspond-
238 ing to $([\text{FeTPPBipy}]^{\bullet})_n$. This is in accordance with the significant

rate of amorphization observed by X-ray diffraction (Figure S3, Supporting Information). Isomer shift (δ) and quadrupolar splitting (ΔE) values are 0.337(1) and 1.054(2) for the first signal and 0.235(2) and 0.326(7) for the second one, in the range usually observed for Fe^{III} ions (Figure 5).

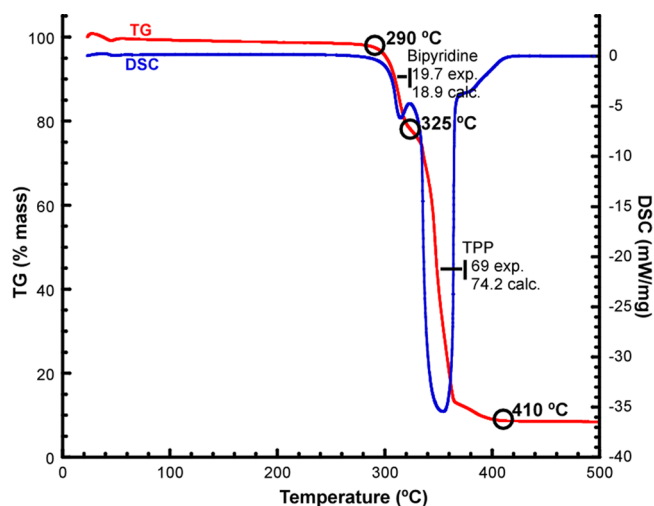


Figure 5. Mössbauer spectra for $([\text{FeTPPbipy}]^\bullet)_n$.

Thermogravimetry. Thermogravimetry analysis was carried out on nonground single crystals. The thermogravimetric decomposition curve of the compound shows an overlapped two-stage mass loss, from approximately 290 to 410 °C. As shown in Figure 6, the first step occurs between 290 and 325 °C with a

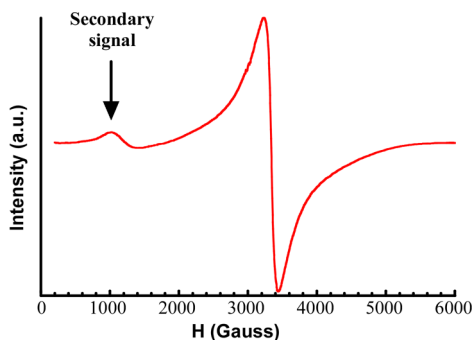


Figure 6. Thermal analysis for $([\text{FeTPPbipy}]^\bullet)_n$.

19.7% weight loss and the second step from 325 to 410 °C with a 69% weight loss. These mass percentages are close to the theoretical percentages of bipyridine (18.9%) and TPP (74.2%) molecules. The calcination product was identified by powder X-ray diffraction analysis, and it consists of Fe₂O₃ [space group $R\bar{3}c$, $a = 5.0248$ Å, $c = 13.7163$ Å, and $\gamma = 120^\circ$].⁵¹

Magnetic Measurements. We have also performed magnetic susceptibility (χ_m) measurements for $([\text{FeTPPbipy}]^\bullet)_n$ in the range 4–300 K (Figure 7). It is worth mentioning that nonground single crystals were used for this analysis, but the original crystals were introduced into a capillary. The $\chi_m T$ value at room temperature is 0.30 cm³ K mol⁻¹, which is much lower than the 4.37 cm³ K mol⁻¹ value expected for a high-spin Fe^{III} compound. On the contrary, it is close to the 0.37 cm³ K mol⁻¹ value expected for low-spin Fe^{III} complexes. As explained below (DFT calculations), the one-electron reduction of metalloporphyrin is analyzed, with the acquired electrons having been determined to

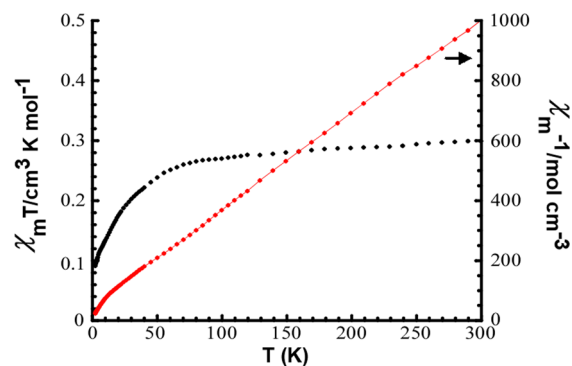


Figure 7. Thermal evolution of $\chi_m T$ and χ_m^{-1} for $([\text{FeTPPbipy}]^\bullet)_n$ and the corresponding theoretical Curie–Weiss law (red line).

be located on the phenyl groups. On the other hand, TD-DFT calculations carried out to analyze the UV–visible spectroscopy (Figure 3b) indicate that there is an important charge transfer between the phenyl rings and metal centers (Figure 3b). Thus, the slight discrepancy between the expected (0.30 cm³ K mol⁻¹) and observed (0.37 cm³ K mol⁻¹) $\chi_m T$ values for low-spin Fe^{III} can be explained if considering this charge transfer.

The thermal evolution of the reciprocal susceptibility follows the Curie–Weiss law with $C_m = 0.32$ cm³ K mol⁻¹ and $\theta = -18.7$ K (Figure 7). The product $\chi_m T$ continuously decreases upon cooling, reaching a value of 0.09 cm³ K mol⁻¹ at 5.0 K, indicating the presence of antiferromagnetic interactions, as expected from EPR characterization. As mentioned, these interactions cannot be attributed to magnetic exchange between metal centers. Therefore, coupling between metal ions and free electrons should be admitted.

DFT Calculations. As previously mentioned, the structural characterization of this compound could make one think that the metal ion is Fe^{II}, in accordance with the presence of TPP²⁻ ligands and neutral bipy molecules. However, the commercial reactant, [FeTPPCL], contains Fe^{III}, and its reduction to Fe^{II} does not seem to be feasible. On the other hand, the bond distances and angles are typical for iron(III) porphyrins, and the rest of the characterization techniques clearly indicate that the metal ion is Fe^{III}. Therefore, the best of our hypothesis is that the compound has been formed by the assembly of $([\text{FeTPP}]^\bullet)$ radical structural units, which extend, producing 1D polymers by means of the axial coordination of the metal center to bipy ligands. Thus, the $([\text{FeTPP}]^\bullet)$ structural units should be thought of as being the result of one-electron reduction of the metalloporphyrin (reactions 1 and 2).



Admitting that reduction must have taken place for the metalloporphyrin, we tried to identify the reductant agent. Even if there are some calculated redox potentials in the literature,⁵² they are not useful in our case because of the nonstandard conditions for solvothermal synthesis. Even so, there are several possible reductant agents like residues of bipy and DMF.⁵³

Thus, next question about $([\text{FeTPPbipy}]^\bullet)_n$ consists of determining the localization of the electron providing the metalloporphyrins with its radical nature. In the case of $([\text{FeTPPbipy}]^\bullet)_n$, the presence of low-spin Fe^{III} and an extra unpaired electron should result in two unpaired electrons per metalloporphyrin. Therefore, we could think of two explanations. As previously proposed,⁵⁴ the extra unpaired electron could be delocalized on the aromatic

Scheme 1. Possibilities for the Number of Unpaired Electrons Depending on the Occurrence of Antiferromagnetic Coupling through π Stacking

	Possible interactions between 1D polymers per two Fe ^{III} centers				π -stacking producing antiferromagnetic interactions
	1D polymer 1		1D polymer 2		
	Fe	TPP	TPP	Fe	
4 unpaired electrons per two Fe ^{III} centers	↑	↑	↑	↑	No
2 unpaired electrons per two Fe ^{III} centers	↓	↑↓		↑	Yes

porphyrinic system. If analysis of the compound is done from the point of view of isolated structural units (1D polymers), this could be an effective explanation. However, magnetic measurements are not consistent with the latter. Besides, there is an intricate π -stacking system in $([\text{FeTPPbipy}]^{\bullet})_n$ according to which analysis of the framework from such a point of view does not seem to be adequate. Thus, a second explanation is that the electrons acquired by reduction are paired in the 3D framework (Scheme 1). This idea is strongly supported by π stacking because it provides the opportunity of electron coupling.

In order to provide theoretical support to the above-mentioned aspects, both hypotheses were analyzed by means of quantum-mechanical DFT calculations (*Gaussian 03* program).⁴⁷ Calculations were performed using Becke's three-parameter hybrid functional with the correlation functional of Lee, Yang, and Parr (B3LYP)^{48,49} with a split-valence basis set of 6-31G. This functional does not consider the dispersive interactions. However, it has been selected because our objective was not obtaining an accurate value for the energy but representative values for a comparison between both hypotheses. In fact, the goal was to investigate the effect of π stacking on the stability of the framework. To this purpose, two dimeric fragments (FeTPPbipy_2) were selected. In dimer 1, the interdimer connection is due to the *edge-to-face* π bond along the [10-1] direction, while in dimer 2, the connection takes place by the *face-to-face* π bond along the [101] direction (Figure 8a). For each dimer, two calculations (Table 3) were carried out: in calculation 1, the dimer has four unpaired electrons (two per monomer), and in calculation 2, the dimer has two unpaired electrons (one per monomer). Therefore, calculation 1 accounts for the first hypothesis (that is, analysis from the point of view of isolated 1D polymers), while calculation 2 explores the possibility of electron coupling through interpolymer π stacking. Obviously, extension of the framework through the three directions of space should have been considered for more accurate calculations. However, the large amount of atoms involved makes this very expensive.

Table 3 summarizes the as-calculated values. As observed, the values show that for both dimers the situation with one unpaired electron per monomer (two per dimer) is more stable than the situation with two unpaired electrons per monomer (four per dimer), supporting the idea that π stacking is responsible for stabilization of the framework.

At this point of the discussion, claiming that π stacking is responsible for stabilization of the framework seems to be obvious. Nevertheless, the remarkable point is that calculations strongly support the idea that the extra electrons have not been delocalized on the TPP pyrrolic system but they are paired in molecular orbitals formed by π stacking. In fact, as observed in Figure 8b,c, the calculations provided molecular orbitals for these interactions.

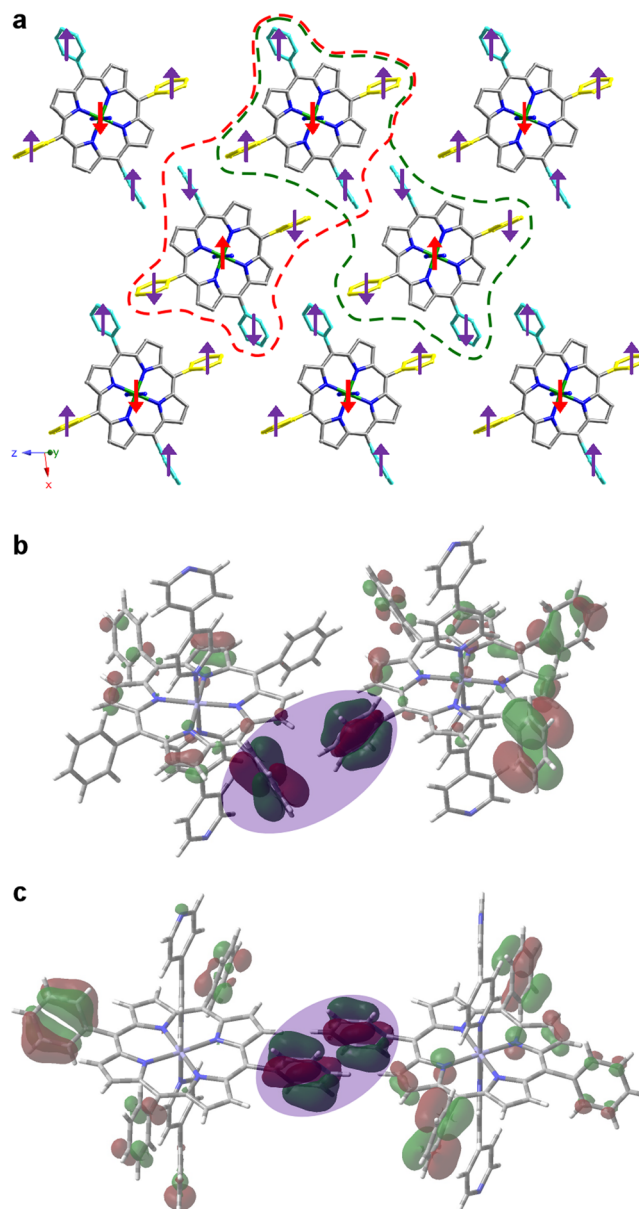


Figure 8. (a) Selected dimeric fragments for the DFT calculations according to *edge-to-face* (red line) and *face-to-face* (green line) π interactions. A scheme for the spin distribution proposal is also shown: red arrows are the unpaired electrons corresponding to low-spin Fe^{III} (d^5), and each group of four purple arrows corresponds to a single electron localized on the phenyl groups belonging to the same metalloporphyrin. (b) Calculated molecular orbitals involving the *edge-to-face* and (c) *face-to-face* π stackings.

Table 3. Calculated Energy for (FeTPPbipy)₂ Dimers

dimer	π interactions	coupling through π interactions	no. of unpaired electrons per dimer	calculated energy (hartree)
1	edge-to-face	yes	2	-8331.1805358
1	edge-to-face	no	4	-8331.1309928
2	face-to-face	yes	2	-8331.1814716
2	face-to-face	no	4	-8331.1533709

Self-Assembly of Neutral Radicals. As π stacking is extended on the (101) planes, extrapolation of the DFT calculations to the 3D network can be done. As observed in Figure 8b,c, the contribution of the phenyl molecular orbitals to π stacking is consistent with this extrapolation. First of all, the electron acquired by the porphyrin could be thought of as delocalized on the four phenyl groups. On the other hand, if considering that magnetic measurements are consistent with the presence of a value close to one unpaired electron per monomer, the spin distribution proposed in Figure 8a could be a reasonable explanation for the behavior of this compound. This spin distribution is based on the occurrence of antiferromagnetic coupling not only between electrons belonging to the metal center and phenyl groups (as previously mentioned in the Magnetic Measurements section) but also between phenyl electrons localized on adjacent 1D polymers, as seen in Figure 8b,c. In summary, identification of the localization of the acquired electrons is the key point that supports the idea of neutral radicals having been able to self-assemble, producing such a 3D framework.

CONCLUSIONS

The compound $[(\text{FeTPPbipy})^*]_n$ has been formed by the assembly of metalloporphyrinic neutral radicals that have been formed by one-electron reduction of the original $[\text{FeTPP}]^+$ cations, as suggested by the presence of low-spin Fe^{III} ions. The as-acquired electrons are proposed to be paired in the molecular orbitals formed by π - π interactions between the phenyl groups of different 1D polymers. The resulting packing is the first Fe-TPP-bipy coordination network exhibiting 1D polymers.

ASSOCIATED CONTENT

Supporting Information

ORTEP detail of the structure, IR and EPR spectra, X-ray measurements, crystallographic data, and a CIF file for CCDC 888109. This material is available free of charge via the Internet at <http://pubs.acs.org>.

AUTHOR INFORMATION

Corresponding Author

*E-mail: gotzone.barandika@ehu.es.

Author Contributions

The manuscript was written through contributions of all authors. All authors have given approval to the final version of the manuscript. All authors contributed equally.

Notes

The authors declare no competing financial interest.

ACKNOWLEDGMENTS

This work has been financially supported by the "Ministerio de Ciencia e Innovación" (MAT2010-15375), the "Gobierno Vasco" (Basque University System Research Groups, IT-630-13), and UPV/EHU (UFI 11/15), which we gratefully acknowledge. SGlker (UPV/EHU) technical support (MEC, GV/EJ, European Social

Fund) is gratefully acknowledged. The authors thank Dr. Fernando Plazaola (UPV/EHU) for her help in interpreting the Mössbauer spectra. A.F.-M. thanks the UPV/EHU for fellowships.

REFERENCES

- Beletskaya, I.; Tyurin, V. S.; Tsivadze, A. Y.; Guillard, R.; Stern, C. *Chem. Rev.* **2009**, *109*, 1659–1713.
- Drain, C. M.; Varotto, A.; Radivojevic, I. *Chem. Rev.* **2009**, *109*, 1630–1658.
- Wang, C.; Xie, Z.; deKrafft, K. E.; Lin, W. *J. Am. Chem. Soc.* **2011**, *133*, 13445–13454.
- Margelefsky, E. L.; Zeidan, R. K.; Davis, M. E. *Chem. Soc. Rev.* **2008**, *37*, 1118–1126.
- Mola, J.; Mas-Marza, E.; Sala, X.; Romero, I.; Rodriguez, M.; Vinas, C.; Parella, T.; Llobet, A. *Angew. Chem., Int. Ed.* **2008**, *47*, 5830–5832.
- Zou, C.; Wu, C.-D. *Dalton Trans.* **2012**, *41*, 3879–3888.
- Shultz, A. M.; Farha, O. K.; Hupp, J. T.; Nguyen, S. T. *J. Am. Chem. Soc.* **2009**, *131*, 4204–4205.
- Gao, B.; Zhao, J.; Li, Y. *J. Appl. Polym. Sci.* **2011**, *122*, 406–416.
- Mohnani, S.; Bonifazi, D. *Coord. Chem. Rev.* **2010**, *254*, 2342–2362.
- Zeitouny, J.; Aurisicchio, C.; Bonifazi, D.; De Zorzi, R.; Geremia, S.; Bonini, M.; Palma, C.-A.; Samori, P.; Listorti, A.; Belbakra, A.; Armaroli, N. *J. Mater. Chem.* **2009**, *19*, 4715–4724.
- Liu, C.-X.; Liu, Q.; Guo, C.-C.; Tan, Z. *J. Porphyrins Phthalocyanines* **2010**, *14*, 825–831.
- Castro, K. A. D. F.; Halma, M.; Machado, G. S.; Ricci, G. P.; Ucoski, G. M.; Ciuffi, K. J.; Nakagaki, S. *J. Braz. Chem. Soc.* **2010**, *21*, 1329–1340.
- Serwicka, E. M.; Poltowicz, J.; Bahranowski, K.; Olejniczak, Z.; Jones, W. *Appl. Catal., A* **2004**, *275*, 9–14.
- Schuenemann, V.; Trautwein, A. X.; Rietjens, I. M. C. M.; Boersma, M. G.; Veeger, C.; Mandon, D.; Weiss, R.; Bahl, K.; Colapietro, C.; Piech, M.; Austin, R. N. *Inorg. Chem.* **1999**, *38*, 4901–4905.
- Cooke, P. R.; Gilmartin, C.; Gray, G. W.; Lindsay Smith, J. R. *J. Chem. Soc., Perkin Trans. 2* **1995**, *2*, 1573–1578.
- Hilal, H. S.; Kim, C.; Sito, M. L.; Schreiner, A. F. *J. Mol. Catal.* **1991**, *64*, 133–142.
- Garibay, S. J.; Stork, J. R.; Cohen, S. M. *Prog. Inorg. Chem.* **2009**, *56*, 335–378.
- Burnett, B. J.; Barron, P. M.; Choe, W. *CrystEngComm* **2012**, *14*, 3839–3846.
- Kumar, R. K.; Balasubramanian, S.; Goldberg, I. *Chem. Commun.* **1998**, 1435–1436.
- Tsao, T.-B.; Lee, G.-H.; Yeh, C.-Y.; Peng, S.-M. *Dalton Trans.* **2003**, 1465–1471.
- Kumar, D. K.; Das, A.; Dastidar, P. *Inorg. Chem.* **2007**, *46*, 7351–7361.
- Diskin-Posner, Y.; Patra, G. K.; Goldberg, I. *J. Chem. Soc., Dalton Trans.* **2001**, 2775–2782.
- Wang, Q.-G.; Xie, Y.-S.; Zeng, F.-H.; Ng, S.-W.; Zhu, W.-H. *Inorg. Chem. Commun.* **2010**, *13*, 929–931.
- Burrell, A. K.; Officer, D. L.; Reid, D. C. W.; Wild, K. Y. *Angew. Chem., Int. Ed.* **1998**, *37*, 114–117.
- Mikami, S.; Sugiura, K.-i.; Maruta, T.; Maeda, Y.; Ohba, M.; Usuki, N.; Okawa, H.; Akutagawa, T.; Nishihara, S.; Nakamura, T.; Iwasaki, K.; Miyazaki, N.; Hino, S.; Asato, E.; Miller, J. S.; Sakata, Y. *J. Chem. Soc., Dalton Trans.* **2001**, 448–455.
- Summerville, D. A.; Cohen, I. A.; Hatano, K.; Scheidt, W. R. *Inorg. Chem.* **1978**, *17*, 2906–2910.
- Calderon-Casado, A.; Barandika, G.; Bazan, B.; Urtiaga, M.-K.; Vallcorba, O.; Rius, J.; Miravittles, C.; Arriortua, M.-I. *CrystEngComm* **2011**, *13*, 6831–6838.
- Barandika, M. G.; Hernandez-Pino, M. L.; Urtiaga, M. K.; Cortes, R.; Lezama, L.; Arriortua, M. I.; Rojo, T. *J. Chem. Soc., Dalton Trans.* **2000**, 1469–1473.

- 475 (29) Barandika, M. G.; Cortes, R.; Serna, Z.; Lezama, L.; Rojo, T.;
476 Urutiaga, M. K.; Arriortua, M. I. *Chem. Commun.* **2001**, 45–46.
- 477 (30) de la Pinta, N.; Martin, S.; Urutiaga, M. K.; Barandika, M. G.;
478 Arriortua, M. I.; Lezama, L.; Madariaga, G.; Cortes, R. *Inorg. Chem.*
479 **2010**, *49*, 10445–10454.
- 480 (31) Hernandez, M. L.; Urutiaga, M. K.; Barandika, M. G.; Cortes, R.;
481 Lezama, L.; de la Pinta, N.; Arriortua, M. I.; Rojo, T. *J. Chem. Soc., Dalton*
482 *Trans.* **2001**, 3010–3014.
- 483 (32) Serna, Z. F.; Lezama, L.; Urutiaga, M. K.; Arriortua, M. I.;
484 Barandika, M. G.; Cortes, R.; Rojo, T. *Angew. Chem., Int. Ed.* **2000**, *39*,
485 344–347.
- 486 (33) Fidalgo-Marijuan, A.; Barandika, G.; Bazan, B.; Urutiaga, M.-K.;
487 Arriortua, M.-I. *Polyhedron* **2011**, *30*, 2711–2716.
- 488 (34) DeVries, L. D.; Choe, W. *J. Chem. Crystallogr.* **2009**, *39*, 229–240.
- 489 (35) Yinghua, W. *J. Appl. Crystallogr.* **1987**, *20*, 258–259.
- 490 (36) Sheldrick, G. M. *Acta Crystallogr., Sect. A: Found. Crystallogr.* **2008**,
491 *A64*, 112–122.
- 492 (37) Scheidt, W. R.; Geiger, D. K.; Haller, K. J. *J. Am. Chem. Soc.* **1982**,
493 *104*, 495–499.
- 494 (38) Saffari, J.; Khorasani-Motlagh, M.; Noroozifar, M. *Synth. React.*
495 *Inorg., Met.–Org., Nano-Met. Chem.* **2010**, *40*, 899–904.
- 496 (39) Mezger, M.; Hanack, M.; Hirsch, A.; Kleinwaechter, J.; Mangold,
497 K. M.; Subramanian, L. R. *Chem. Ber.* **1991**, *124*, 841–847.
- 498 (40) Jentzen, W.; Song, X.-Z.; Shelnut, J. A. *J. Phys. Chem. B* **1997**, *101*,
499 1684–1699.
- 500 (41) Jentzen, W.; Ma, J.-G.; Shelnut, J. A. *Biophys. J.* **1998**, *74*, 753–
501 763.
- 502 (42) Ohgo, Y.; Hoshino, A.; Okamura, T.; Uekusa, H.; Hashizume, D.;
503 Ikezaki, A.; Nakamura, M. *Inorg. Chem.* **2007**, *46*, 8193–8207.
- 504 (43) Quinn, R.; Strouse, C. E.; Valentine, J. S. *Inorg. Chem.* **1983**, *22*,
505 3934–3940.
- 506 (44) Ikezaki, A.; Tukada, H.; Nakamura, M. *Chem. Commun.* **2008**,
507 2257–2259.
- 508 (45) Gans, P.; Buisson, G.; Duee, E.; Marchon, J. C.; Erler, B. S.;
509 Scholz, W. F.; Reed, C. A. *J. Am. Chem. Soc.* **1986**, *108*, 1223–1234.
- 510 (46) Ochiai, E.-i. *Bioinorganic Chemistry: An Introduction*; Allyn and
511 Bacon, Inc.: Boston, MA, 1977; Chapter 5.
- 512 (47) Frisch, M. J.; Trucks, G. W.; Schlegel, H. B.; Scuseria, G. E.; Robb,
513 M. A.; Cheeseman, J. R.; Montgomery, J. A., Jr.; Vreven, T.; Kudin, K.
514 N.; Burant, J. C.; Millam, J. M.; Iyengar, S. S.; Tomasi, J.; Barone, V.;
515 Mennucci, B.; Cossi, M.; Scalmani, G.; Rega, N.; Petersson, G. A.;
516 Nakatsuji, H.; Hada, M.; Ehara, M.; Toyota, K.; Fukuda, R.; Hasegawa,
517 J.; Ishida, M.; Nakajima, T.; Honda, Y.; Kitao, O.; Nakai, H.; Klene, M.;
518 Li, X.; Knox, J. E.; Hratchian, H. P.; Cross, J. B.; Bakken, V.; Adamo, C.;
519 Jaramillo, J.; Gomperts, R.; Stratmann, R. E.; Yazyev, O.; Austin, A. J.;
520 Cammi, R.; Pomelli, C.; Ochterski, J. W.; Ayala, P. Y.; Morokuma, K.;
521 Voth, G. A.; Salvador, P.; Dannenberg, J. J.; Zakrzewski, V. G.; Dapprich,
522 S.; Daniels, A. D.; Strain, M. C.; Farkas, O.; Malick, D. K.; Rabuck, A. D.;
523 Raghavachari, K.; Foresman, J. B.; Ortiz, J. V.; Cui, Q.; Baboul, A. G.;
524 Clifford, S.; Cioslowski, J.; Stefanov, B. B.; Liu, G.; Liashenko, A.;
525 Piskorz, P.; Komaromi, I.; Martin, R. L.; Fox, D. J.; Keith, T.; Al-Laham,
526 M. A.; Peng, C. Y.; Nanayakkara, A.; Challacombe, M.; Gill, P. M. W.;
527 Johnson, B.; Chen, W.; Wong, M. W.; Gonzalez, C.; Pople, J. A. *Gaussian*
528 *03*, revision D.02; Gaussian, Inc.: Wallingford, CT, 2004.
- 529 (48) Becke, A. D. *J. Chem. Phys.* **1993**, *98*, 5648–5652.
- 530 (49) Lee, C.; Yang, W.; Parr, R. G. *Phys. Rev. B: Condens. Matter* **1988**,
531 *37*, 785–789.
- 532 (50) Brand, R. A.; Lauer, J.; Herlach, D. M. *J. Phys. F: Met. Phys.* **1983**,
533 *13*, 675–683.
- 534 (51) Tsirel'son, V. G.; Antipin, M. Y.; Strel'tsov, V. A.; Ozerov, R. P.;
535 Struchkov, Y. T. *Dokl. Akad. Nauk SSSR* **1988**, *298*, 1137–1141.
- 536 (52) Ou, Z.; E, W.; Zhu, W.; Thordarson, P.; Sintic, P. J.; Crossley, M.
537 J.; Kadish, K. M. *Inorg. Chem.* **2007**, *46*, 10840–10849.
- 538 (53) Pereira, M. M.; Abreu, A. R.; Goncalves, N. P. F.; Calvete, M. J. F.;
539 Simoes, A. V. C.; Monteiro, C. J. P.; Arnaut, L. G.; Eusebio, M. E.;
540 Canotilho, J. *Green Chem.* **2012**, *14*, 1666–1672.
- 541 (54) Scheidt, W. R.; Brancato-Buentello, K. E.; Song, H.; Reddy, K. V.;
542 Cheng, B. *Inorg. Chem.* **1996**, *35*, 7500–7507.

“This document is the Accepted Manuscript version of a Published Work that appeared in final form in *Inorganic Chemistry*, copyright © American Chemical Society after peer review and technical editing by the publisher. To access the final edited and published work see <http://http://pubs.acs.org/doi/abs/10.1021/ic4007372>.”